JOURNAL OF GEOPHYSICAL RESEARCH, VOL. 115, D00J06, doi:10.1029/2009JD013313, 2010

Comparison of GOES-retrieved and in situ measurements of deep convective anvil cloud microphysical properties during the Tropical Composition, Cloud and Climate Coupling Experiment (TC^4)

Christopher R. Yost,[1] Patrick Minnis,[2] J. Kirk Ayers,[1] Douglas A. Spangenberg,[1] Andrew J. Heymsfield,[3] Aaron Bansemer,[3] Matthew J. McGill,[4] and Dennis L. Hlavka[5]

Received 30 September 2009; revised 22 February 2010; accepted 17 March 2010; published 21 July 2010.

[1] One of the main goals of the Tropical Composition, Cloud and Climate Coupling Experiment (TC^4) during July and August 2007 was to gain a better understanding of the formation and life cycle of cirrus clouds in the upper troposphere and lower stratosphere and how their presence affects the exchange of water vapor between these layers. Additionally, it is important to compare in situ measurements taken by aircraft instruments with products derived from satellite observations and find a meaningful way to interpret the results. In this study, cloud properties derived using radiance measurements from the Geostationary Operational Environmental Satellite (GOES) imagers are compared to similar quantities from aircraft in situ observations and are examined for meaningful relationships. A new method using dual-angle satellite measurements is used to derive the ice water content (IWC) for the top portion of deep convective clouds and anvils. The results show the in situ and remotely sensed mean microphysical properties agree to within ~10 μm in the top few kilometers of thick anvils despite the vastly different temporal and spatial resolutions of the aircraft and satellite instruments. Mean particle size and IWC are shown to increase with decreasing altitude in the top few kilometers of the cloud. Given these relationships, it may be possible to derive parameterizations for effective particle size and IWC as a function of altitude from satellite observations.

Citation: Yost, C. R., P. Minnis, J. K. Ayers, D. A. Spangenberg, A. J. Heymsfield, A. Bansemer, M. J. McGill, and D. L. Hlavka (2010), Comparison of GOES-retrieved and in situ measurements of deep convective anvil cloud microphysical properties during the Tropical Composition, Cloud and Climate Coupling Experiment (TC^4), *J. Geophys. Res.*, *115*, D00J06, doi:10.1029/2009JD013313.

1. Introduction

[2] Clouds play a key role in Earth's radiation budget and hydrological cycle. The horizontal and vertical distribution of cloud water affects atmospheric and surface heating rates as well as the distribution of precipitation. Accurate determination of the 3-D cloud field for a given domain is important, not only for understanding the role of clouds in weather and climate, but also for guiding the development and refinement of cloud process models and for use in initializing forecast models [e.g., *Benjamin et al.*, 2004]. Active remote sensing instruments such as lidars and radars can provide vertical profiles of cloud hydrometeor concentrations [e.g., *Dong et al.*, 2002; *Wang and Sassen*, 2002] and layering. Until the last few years, such information has been available only from fixed surface locations and limited aircraft measurements during field experiments. The launch of the Cloud-Aerosol Lidar and Infrared Pathfinder Satellite Observations (CALIPSO) satellite [*Winker et al.*, 2007] and CloudSat [*Stephens et al.*, 2008] have placed a cloud lidar and radar, respectively, into space producing global measurements of cloud vertical profiles. Yet, even with such advances, the active sensors still provide only cross sections of the 3-D cloud fields at either two specific times of day (satellites) or at a single point on Earth. Passive radiance measurements, limited as they are, remain necessary for taking measurements over all locations at all times of day. Scanning active sensors for observing clouds from a geostationary orbit are unlikely to be launched in the near future. Thus, it is important to continue researching new techniques for extracting 3-D cloud information from satellite imagers.

[3] Recent advances in retrieving 3-D cloud information from passive imagery have resulted in multispectral methods

[1]Science Systems and Applications, Inc., Hampton, Virginia, USA.
[2]NASA Langley Research Center, Hampton, Virginia, USA.
[3]National Center for Atmospheric Research, Boulder, Colorado, USA.
[4]NASA Goddard Space Flight Center, Greenbelt, Maryland, USA.
[5]Science Systems and Applications, Inc., Greenbelt, Maryland, USA.

0148-0227/10/2009JD013313

for deriving profiles of cloud particle sizes [e.g., *Wang et al.*, 2009] and for detecting multilayered clouds and retrieving their cloud properties [e.g., *Chang et al.*, 2010]. *Minnis et al.* [2008] used a combination of CALIPSO and Aqua Moderate Resolution Imaging Spectroradiometer (MODIS) data to improve the estimation of the physical cloud top heights of optically thick ice clouds from infrared brightness temperature measurements, a quantity that has been subject to significant biases [e.g., *Sherwood et al.*, 2004]. In the course of that analysis, *Minnis et al.* [2008] suggested that it should be possible to retrieve ice water content (IWC) for the upper 2 km of optically thick ice clouds using passive radiance measurements from two satellite observations taken at different viewing zenith angles (VZA). The proposed method has yet to be tested. Knowing the IWC at the top of thick clouds might also be valuable for estimating the vertical distribution of IWC throughout the clouds, especially if used in conjunction with a technique like that of *Wang et al.* [2009] for profiling the effective particle sizes within the cloud.

[4] The Tropical Composition, Cloud and Climate Coupling Experiment (TC^4) [*Toon et al.*, 2010] conducted from San Jose, Costa Rica during summer 2007 provides an opportunity for examining the new methods for inferring cloud top IWC and validating retrievals of ice particle size and water path for deep convective clouds in the tropics during daytime. Being designed to study convectively generated cirrus clouds and transport of water vapor into the tropical tropopause layer (TTL), TC^4 conducted numerous flights both within and above deep convective clouds. Cloud top height and vertical profiles of cirrus clouds were observed with a high-altitude down-looking lidar, while in situ instruments measured particle sizes and IWC. In this paper, the dual-angle technique for retrieving IWC in the cloud tops is developed and applied to Geostationary Operational Environmental Satellite (GOES) data. The retrievals of IWC, cloud ice crystal effective size, and ice water path (IWP) are examined by comparing with the aircraft-based measurements of the same quantities. The results are discussed in light of the complexities of the cloud systems and the limitations of observational consistency among the measurements. The analysis should provide a better estimate of how these new methods can resolve parts of the 3-D cloud structure.

2. Data

[5] The Tenth and Twelfth Geostationary Operational Environmental Satellites (GOES-10/12) provided valuable radiance measurements over the entire TC^4 domain for the duration of the experiment. GOES-10 and GOES-12 are situated on the Equator at 60°W and 75°W, respectively, and have a nominal spatial resolution of 4 km at nadir. Four spectral channels are common to both satellites: visible (VIS, 0.65 μm), shortwave infrared (SIR, 3.9 μm), water vapor (WV, 6.7 μm), and infrared (IR, 10.8 μm). The fifth channels on GOES-10 and 12 are the split window (SPW, 12.0 μm) and CO2-slicing (COS, 13.3 μm, 8 km resolution), respectively. GOES imagery typically had temporal resolution of 15–30 min over the TC^4 domain.

[6] The NASA DC-8 aircraft, managed during TC^4 by the University of North Dakota, was equipped with an array of sensors designed to take remote and in situ measurements of clouds, aerosols, and gases [*Toon et al.*, 2010]. The aircraft is capable of flights to an altitude of 12 km for durations exceeding 10 h and made a total of 13 science flights during TC^4. The DC-8 flew through both low- and high-level clouds taking measurements at different levels within clouds and occasionally obtaining profiles of various properties from cloud top to base. Of particular interest for this study are measurements of cloud particle size and frozen water content. During TC^4, the DC-8 was equipped with two cloud probes, the two-dimensional cloud-imaging probe (2D-CIP) and precipitation-imaging probe (2D-PIP), designed to measure the size of cloud and precipitation particles. Combined, CIP and PIP, simply referred to hereafter as CIP, have a dynamic range of 25–6400 μm and resolutions of 25 and 100 μm, respectively [*Kingsmill et al.*, 2004].

[7] The NASA ER-2 high-altitude aircraft flew a total of 13 science flights during TC^4 carrying a variety of remote sensors. Among these sensors was the Cloud Physics Lidar (CPL), an active remote sensor designed to take multispectral measurements of cirrus, subvisual cirrus, and aerosols with high temporal and spatial resolution [*McGill et al.*, 2002]. Measurements of backscatter from the 355, 532, and 1064 nm channels are used to determine the altitude and optical depth of up to 10 cloud or aerosol layers. The lidar beam is completely attenuated by features with optical depths greater than ~3 and is unable to detect cloud and aerosol features beyond this limit. Because of its sensitivity to weakly scattering particles, high temporal and spatial resolution, and range-resolving ability, the CPL is a valuable instrument for validating cloud top heights derived from passive satellite radiance measurements.

3. Methodology

[8] Aircraft instruments often measure cloud properties that are not directly comparable to quantities derived from satellite instruments. Typically, they measure instantaneous quantities that may vary significantly in time and space while passive spaceborne sensors usually provide column-integrated quantities. In the case of optically thick anvils, satellite derived cloud properties tend to be representative of conditions near cloud top while aircraft are capable of profiling the entire cloud. In section 3, we describe methods to derive quantities from aircraft and satellite observations that are more analogous to each other. This makes the comparison of aircraft- and satellite-derived cloud properties a more feasible task.

3.1. Satellite Retrievals

[9] All satellite cloud properties in this study were derived from GOES data as described by P. Minnis et al. (Cloud properties determined from GOES and MODIS data during TC^4, unpublished manuscript, 2009). During daytime, defined as solar zenith angle (SZA) < 82°, the visible-infrared-shortwave-infrared-split-window technique (VISST) is used to retrieve cloud properties including cloud effective temperature T_{eff}, effective cloud height Z_{eff}, cloud top height Z_t, thermodynamic phase (water or ice), optical depth τ, effective droplet radius r_e, and effective ice crystal diameter D_e (R. Minnis et al., Cloud property retrievals for CERES using TRMM VIRS and Terra and Aqua MODIS

data, submitted to *IEEE Trans. Geosci. Remote Sens.*). Liquid water path (LWP) and IWP are computed from the effective particle size and optical depth. During TC^4, cloud properties were derived in near-real time from GOES imagery in order to help mission teams plan safe flight routes and maximize success in meeting science objectives (P. Minnis et al., unpublished manuscript, 2009). The data were later reprocessed using a revised set of algorithms and matched temporally and spatially to the flight tracks of the DC-8 and ER-2. Each sampling time from the CIP was matched to the nearest 4 GOES pixels. Because high-altitude clouds can cause slight spatial mismatches when comparing cloud properties, a parallax correction was made when searching for the nearest satellite pixels. Cloud top heights from the CPL were used to make this correction where they were available. Where no CPL data were available, the cloud top height from VISST was used. On 17, 22, and 31 July and 5 and 8 August, the DC-8 and ER-2 coordinated their flight paths and the two planes flew over the same locations within seconds of each other. For these coordinated DC-8 and ER-2 flights, the DC-8 flight track was first matched to the satellite pixels. CIP cloud properties were averaged within a 4 km radius of the DC-8's location in order to obtain mean cloud properties on a spatial scale similar the nominal spatial resolution of GOES. Matched data from the CPL were then found by taking the mean of the properties within 4 km of the location of the DC-8 and within 2 min of the CIP sampling time.

3.2. Computation of D_e

[10] For spherical cloud droplets, size distributions $n(r)$ are expressed as the number of particles n having a radius between r and $r + \Delta r$, where Δr is the width of the size bin. However, ice particles are known to take a variety of shapes that are highly irregular and poorly represented by spheres in radiative transfer calculations [*Yang et al.*, 2003]. Instead, it is common to classify ice crystals by their length or maximum dimension L and the size distribution is therefore expressed as $n(L)$. To be consistent with the VISST cloud retrieval algorithms, we assume that all ice particles are hexagonal columns with length L and width D. *Wyser and Yang* [1998] determined a functional relationship between L and D for the case of hexagonal columns given by $D = 2.5L^{0.6}$. The equation used to compute D_e in this study is

$$D_e = \frac{\int D \times LDn(L)dL}{\int D \times Ln(L)dL}, \tag{1}$$

following *Minnis et al.* [1998]. Computing D_e this way gives a quantity that is analogous to the particle size retrieved from satellite radiance measurements.

3.3. Computation of IWC

[11] In situ measurements from CIP provide estimates of IWC along the path of the airplane, and the VISST estimates IWP over an area including the flight path. These two values are not directly comparable, even if the IWP were uniform over the pixel area, since IWP is a column-integrated quantity. Only occasionally did the DC-8 make spiral descents through clouds to get a full IWC profile, which can then be integrated over the depth of the layer to obtain IWP. However, it may be possible to estimate IWC near cloud top if the proper set of satellite measurements was available. *Sherwood et al.* [2004] and *Minnis et al.* [2008] demonstrated that the physical top of even optically thick ice clouds is underestimated when using a standard IR cloud top retrieval method. Instead, the height retrieved by IR-based methods typically lies 1–2 km below the actual physical top. On the basis of this difference between the physical and radiating top of the cloud, *Minnis et al.* [2008] suggested that IWC could be retrieved from passive radiance measurements given two satellite observations that observe a given scene from different VZAs. IWC is defined as

$$IWC = \frac{2\rho_i \tau D_e}{3Q_e \Delta z}, \tag{2}$$

where ρ_i = 0.9 g cm^{-3} is the bulk density of ice, τ is the optical depth of the cloud layer in the VIS channel, Q_e = 2.0 is the extinction efficiency, and Δz is the physical thickness of the cloud layer. For two satellites viewing the same cloud, there are two retrievals of cloud effective temperature T_{eff1} and T_{eff2} from two different viewing angles θ_1 and θ_2. If $\theta_1 > \theta_2$, then $T_{eff1} < T_{eff2}$ because more of the upper, colder portion of the cloud is along the line-of-sight of the satellite viewing at θ_1, while the one viewing at θ_2 detects more IR radiance from deeper in the cloud, where the temperature should be greater than near cloud top. Thus T_{eff1} will be observed at a higher-altitude Z_{eff1}, in a local temperature sounding than T_{eff2}, observed at altitude Z_{eff2}. If it is assumed that the difference between the heights $\Delta Z_{eff} = Z_{eff1} - Z_{eff2}$ is due entirely to different VZAs, then it is possible to estimate IWC in the cloud layer as represented by ΔZ_{eff} given by

$$IWC = \frac{2\rho_i \Delta\tau D_e}{3Q_e \Delta Z_{eff}}, \tag{3}$$

where

$$\Delta\tau = l(\cos\theta_2 - \cos\theta_1), \tag{4}$$

and $l \approx 1.2$ as discussed in the work of *Minnis et al.* [2008]. The variable, l, is a function only of the single-scattering albedo ω and asymmetry factor g of the ice particles and is given by

$$l = \frac{1}{[3(1-\omega)(1-\omega g)]^{1/2}}. \tag{5}$$

It is referred to by *Coakley and Davies* [1986] as the diffusion length and is a measure of how far photons penetrate a scattering and absorbing medium before being absorbed. Because ω and g are functions of D_e, l varies with D_e also. Figure 1 shows the variability of ω, g, and l with D_e. As expected, l decreases slightly with decreasing particle size since smaller particles have more cross-sectional area for a given IWC resulting in more absorption. Substituting (4) into (3), the equation for IWC becomes

$$IWC = lD_e \frac{2\rho_i}{3Q_e} \frac{\mu_2 - \mu_1}{Z_{eff1} - Z_{eff2}}, \tag{6}$$

where μ_1 and μ_2 are the cosines of θ_1 and θ_2, respectively. In practice, the average value of D_e from the two angles is used in equation (6). It follows that if $\mu_1 = \mu_2$ or $Z_{eff1} = Z_{eff2}$, then

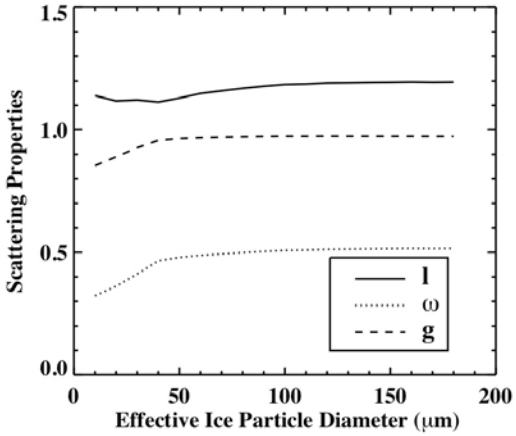

Figure 1. Diffusion length l, single-scattering albedo ω, and asymmetry factor g as a function of effective ice crystal size.

no IWC retrieval is possible. Furthermore, there is more confidence in the retrieval when the difference between μ_1 and μ_2 is not too small. In the following discussion, the quantities $\mu_2 - \mu_1$ and $Z_{eff1} - Z_{eff2}$ are referred to as $\Delta\mu$ and ΔZ_{eff}, respectively, for simplicity. The IWC obtained from various values of $\Delta\mu$, ΔZ_{eff}, and D_e are shown in Figure 2. The range of IWC that can be retrieved with the current method is approximately 0.0001–0.1 g m^{-3}. For small D_e there is little sensitivity to IWC greater than 0.01 g m^{-3} and errors in ΔZ_{eff} of a few hundred meters may cause IWC to be in error by an order of magnitude, particularly when ΔZ_{eff} and $\Delta\mu$ are small (Figure 2a). When $\Delta\mu$ is less than ~0.1 it is almost impossible to reliably retrieve IWC greater than ~0.001 g m^{-3} for any particle size owing to uncertainties in ΔZ_{eff}. Sensitivity to the upper IWC range increases with increasing D_e particularly when $\Delta\mu > 0.20$ (see Figures 2b and 2c). Here, equation (6) is used to retrieve IWC from simultaneous satellite observations near cloud top along the DC-8 flight track. In section 5, this retrieval is compared to in situ measurements taken by the CIP near cloud top.

4. Sensitivity Study

[12] It is important to examine how the retrieval of IWC is impacted by deviations from the underlying assumptions. Equation (6) is based on a simplification of the radiative transfer equation that implicitly assumes that the profile of IWC is constant with altitude. The equation for monochromatic infrared radiative transfer in a nonscattering atmosphere is given more precisely by

$$I_\lambda = B_\lambda(T_{eff}) + \int_{Z_{eff}}^{Z_t} B_\lambda[T(z)]e^{-\tau(z)/\mu}\frac{dz}{\mu}, \qquad (7)$$

where I_λ is the observed monochromatic radiant intensity and B_λ is the Planck function. The second term on the right-hand side of (7) represents thermal emission from cloud layers above Z_{eff}. Because Z_{eff1} and Z_{eff2} are located at different levels within the cloud, and hence are associated with different temperatures, the contribution of thermal emission from the overlying layers is different. This potentially introduces a bias in the denominator of (6), especially if the temperature or IWC profile is strongly stratified. The assumption of constant IWC for a geometrically thin cirrus cloud layer is unrealistic. So too, for geometrically thicker anvil clouds, it is more likely that IWC increases with decreasing altitude from cloud top [e.g., *Seo and Liu*, 2006], but that is not always the case [e.g., *Garrett et al.*, 2005]. It is important to understand how the variation in IWC affects the retrievals.

[13] The sensitivity of retrieved IWC to different IWC profiles was tested using simulated IWC profiles and a layered cloud model. Top-of-atmosphere (TOA) 11.0 μm radiances were computed using the Discrete-Ordinates Radiative Transfer (DISORT) model of *Stamnes et al.* [1988] and a temperature sounding from 3 August 2007, taken near Corozal Oeste, Panama. An ice cloud was inserted between 5.0 and 12.0 km and divided into 475 layers. Twenty-four different IWC profiles were considered. Twelve of the profiles had uniform IWC, 6 decrease linearly with increasing altitude, and 6 increase linearly with increasing altitude. Table 1 gives the IWC values at cloud top and base for each of the profiles along with the total optical depth assuming D_e = 40 μm. TOA radiances were computed for VZA = 0, 5, 10, 15, 20, 30, 40, 50, 60, and 70°.

[14] The computed 11 μm radiances were converted to brightness temperatures and treated as the T_{eff} values that would have been computed by VISST and were converted to Z_{eff} using a fifth-order polynomial fit to the temperature

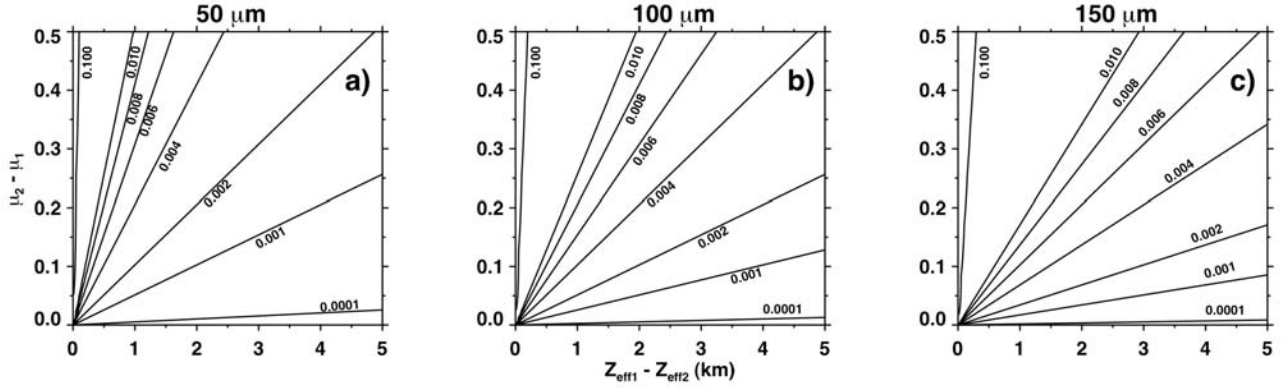

Figure 2. Contour plots of ice water content (g m^{-3}) as a function of $Z_{eff1} - Z_{eff2}$ and $\mu_2 - \mu_1$ for effective particle sizes of (a) 50 μm, (b) 100 μm, and (c) 150 μm.

Table 1. IWC Profile Characteristics Used in DISORT Simulations

Profile Number	Profile Function With Altitude	IWC_{top} (g m^{-3})	IWC_{base} (g m^{-3})	IWC_{ref}	τ_{total}
1	constant	0.001	0.001	0.001	0.58
2	constant	0.003	0.003	0.003	1.75
3	constant	0.005	0.005	0.005	2.90
4	constant	0.007	0.007	0.007	4.07
5	constant	0.009	0.009	0.009	5.24
6	constant	0.01	0.01	0.01	5.82
7	constant	0.02	0.02	0.02	11.63
8	constant	0.03	0.03	0.03	17.45
9	constant	0.05	0.05	0.05	29.09
10	constant	0.10	0.10	0.1	58.17
11	constant	0.20	0.20	0.2	116.34
12	constant	0.50	0.50	0.5	290.86
13	linear decrease	0.00001	0.005	0.002	1.46
14	linear decrease	0.0001	0.01	0.003	2.94
15	linear decrease	0.001	0.1	0.010	29.38
16	linear decrease	0.005	0.2	0.012	30.54
17	linear decrease	0.1	0.4	0.103	145.43
18	linear decrease	0.2	0.6	0.202	232.69
19	linear increase	0.005	0.00001	0.004	1.46
20	linear increase	0.01	0.0001	0.009	2.94
21	linear increase	0.1	0.001	0.099	29.38
22	linear increase	0.2	0.005	0.199	59.63
23	linear increase	0.4	0.1	0.399	145.43
24	linear increase	0.6	0.2	0.599	232.69

sounding used in the computations. The retrieval by the VISST would include a correction for scattering which varies with VZA. The IWC was then computed using (6) while holding one viewing angle constant and varying the second angle, assuming l = 1.1 (see Figure 1). The computed IWC, denoted IWC_{calc}, was compared with a reference IWC, denoted IWC_{ref}, which is the mean IWC in the top layers of the cloud having a cumulative optical depth of 1.1. For the uniform IWC profiles, IWC_{ref} is simply the value of the prescribed IWC. The IWC_{ref} values for all profiles are given in Table 1.

[15] Figure 3 compares the IWC calculated from (6) with the reference IWC. In this case, one viewing angle was held constant at 30° while the second angle was varied. When the IWC profile is uniform, the IWC retrieval using (6) yields overestimates of IWC for $IWC_{ref} < 0.005$, and slight underestimates for IWC_{ref} in the range 0.01–0.1 for most angles (Figure 3a). For larger values of IWC_{ref}, the overestimate increases. For $IWC_{ref} < 0.05$, IWC is overestimated when IWC decreases with altitude and is underestimated for larger values (Figure 3b). For $IWC_{ref} < 0.01$, the retrieved value overestimates IWC_{ref} for all three types of profiles and underestimates when $IWC_{ref} > 0.10$.

[16] For values of $IWC_{ref} < 0.005$ in Figures 3a and 3b, the IWC is overestimated because the clouds are not optically thick and the some of the surface radiance passes through the cloud at smaller VZAs. At larger values of IWC_{ref}, the clouds are optically very thick and scattering becomes more important causing the cloud to appear colder than without scattering. The VISST attempts to account for the scattering, which is included in the DISORT calculations, so it will reduce this effect. When IWC decreases with increasing height (Figure 3b), equation (6) yields an overestimate at intermediate values because the radiance is passing through more layers of smaller IWC values resulting in a value of T_{eff} that is smaller than expected, thereby yielding a larger value of Z_{eff} and larger IWC than expected. In the rare case when the IWC increases with height (Figure 3c), the opposite effect occurs.

5. Results

5.1. Image From 31 July 2007

[17] To provide the large-scale context, Figure 4 shows a composite GOES-10/12 visible-channel image from 1528 UTC, 31 July 2007. A large mesoscale complex developed off Costa Rica's Pacific coast and produced widespread anvil clouds. Plotted over the GOES imagery in red and cyan are the flight tracks of the DC-8 and ER-2, respectively. Between 1330 and 1600 UTC, the DC-8 and ER-2 flew a coordinated flight pattern among these convective cores and anvils. The ER-2 flew over the system at altitudes of ~20 km allowing the CPL to observe the highest cloud tops, while the DC-8 flew directly beneath the ER-2 at altitudes below 12 km taking in situ particle size and IWC measurements.

[18] Cloud properties derived along the aircraft flight track between 1330 and 1600 UTC are summarized in Figure 5. Figure 5a displays the 532 nm backscatter profiles obtained by the CPL aboard the ER-2. Weak molecular scattering is shown as shades of purple while successively stronger scattering owing to clouds is shown as greens,

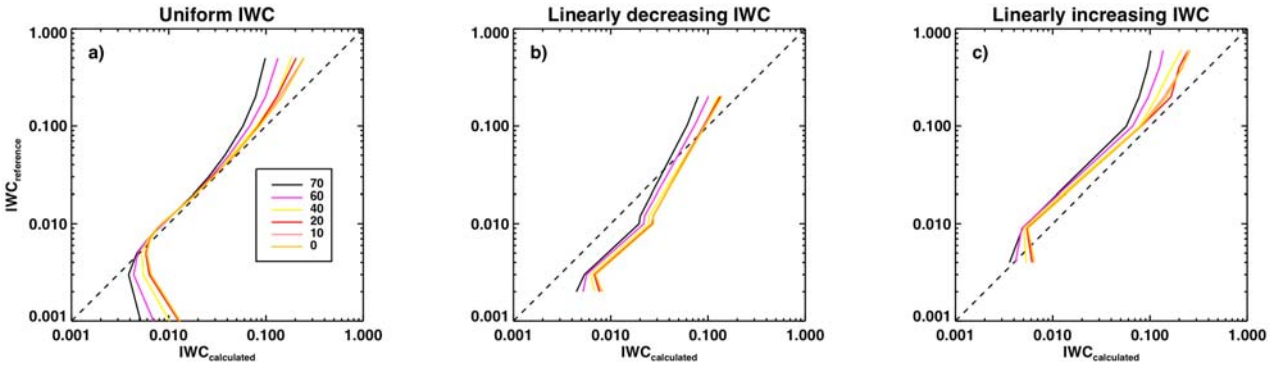

Figure 3. Comparison of IWC_{calc} with IWC_{ref} for (a) uniform, (b) linearly decreasing, and (c) linearly increasing IWC profiles. One viewing angle was held constant at 30° while the second angle was allowed to vary between 0° and 70°.

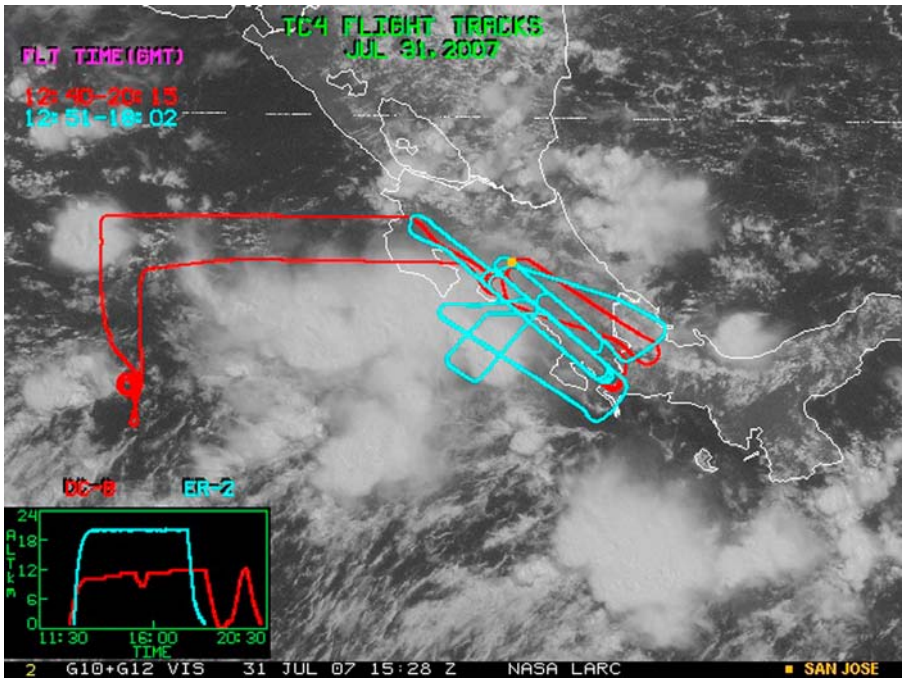

Figure 4. Composite GOES-10/GOES-12 visible image over the TC^4 domain at 1528 UTC on 31 July 2007. The flight tracks of the DC-8 and ER-2 are plotted over the image. Time series of the planes' altitudes are shown in the lower left inset.

blues, reds, and white. Cloud top altitudes are between 15 and 18 km throughout this segment of the flight, well above the altitude of the DC-8. Most of the clouds observed along this segment were thick enough to fully attenuate the lidar beam although optically thin cirrus often overlay the thick anvils, which topped out around 14 km. Complete attenuation of the lidar beam is indicated in Figure 5a as "shadows" beneath strongly scattering features. The aquamarine and red lines in Figure 5a indicate retrievals of Z_{eff} derived by VISST from the GOES-10 and GOES-12 imagery, respectively. Plotted in yellow is the altitude of the DC-8 throughout its flight. On this day, the DC-8 maintained its altitude 4–6 km below the highest anvil top observed by the CPL. The VISST Z_{eff} very closely matches the altitude at which the CPL beam was completely attenuated and VISST Z_t (not shown) lies 1–2 km above Z_{eff}. When the CPL beam is not completely attenuated by thick cirrus and detects both high and low cloud layers such as between 1530 and 1550 UTC, the VISST Z_{eff} and Z_t lie between the two cloud layers. Gaps appear in the VISST cloud heights and DC-8 altitude where the ER-2 briefly deviated from the flight path of the DC-8 and hence no spatially matched data are available. Figure 5b shows the VZAs for GOES-10 and 12. The GOES-10 VZAs were always larger than the GOES-12 VZA by ~15°. The VZA never exceeds 35° for either GOES, so errors introduced by distorted or overlapping pixels owing to extreme viewing angles are expected to be minimal. Figure 5c shows the D_e derived from CIP, GOES-10, and GOES-12 in black, aquamarine, and red, respectively. The GOES retrievals generally follow the same trends, while the D_e values from CIP vary widely as the plane changes altitude within the cloud. Figure 5d shows the IWC retrieved from CIP and GOES-10 and 12. A range of IWC values from <0.0001 g m^{-3} to ~1.0 g m^{-3} is obtained by both methods but those from CIP tend to be much higher, often by an order of magnitude. Although an IWC retrieval was attempted for optically thin and thick clouds, the retrieval should be more reliable for optically thick cirrus and only the thick cirrus are used here. The gray shading in Figure 5 highlights areas where a dual-satellite IWC retrieval was attempted and the cloud optical depth $\tau_c > 8$. The clouds in these regions were also identified as single layer using the CPL data. This is not a completely straightforward task because small gaps are sometimes present between the anvil and overlying thin cirrus. In this situation sometimes two or more cloud layers may be reported by the CPL. For the purposes of this study, a column is only considered multilayered if any cloud layers are detected more than 3 km below the highest cloud top. Any layers detected within 3 km below cloud top are assumed to be part of the same cloud layer. This method eliminates columns where low-level water cloud lies beneath thin cirrus while allowing small gaps to exist in clouds of that are entirely composed of ice particles.

[19] Figures 6a and 6b show scatterplots of D_e estimates from CIP and GOES-10 and GOES-12, respectively. While there is a considerable amount of scatter, the mean difference (CIP minus GOES) between the CIP and GOES estimates of D_e is less than 20 μm. The CIP tends to retrieve larger particle sizes because the DC-8 was flying well below the cloud top and particle size has been shown to increase from cloud top to base [e.g., *Wang et al.*, 2009]. Figure 7 shows the IWC retrievals from GOES-10/12. The in situ IWC is often an order of magnitude greater than the GOES value, probably because IWC is greater deeper in the cloud where the DC-8 was flying. Nevertheless, the CIP and

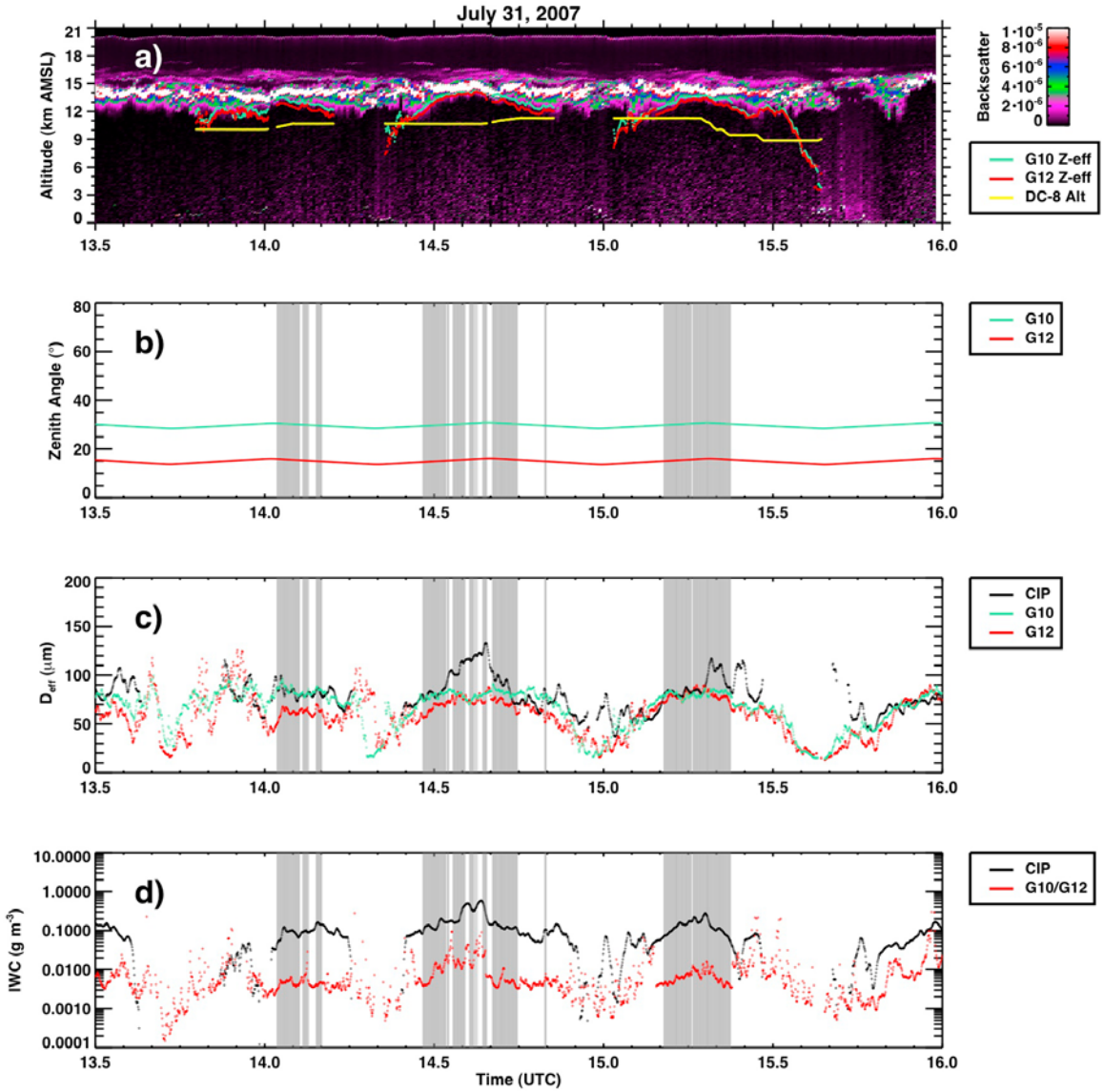

Figure 5. Time series of (a) cloud top, effective radiating, and aircraft altitude plotted over CPL 532 nm backscatter profiles; (b) satellite VZA; (c) effective ice crystal diameter; and (d) ice water content for 31 July 2007.

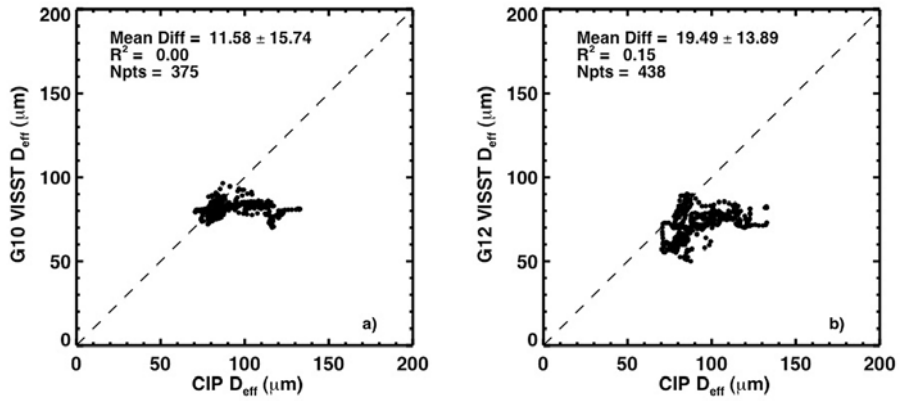

Figure 6. Scatterplots of D_e estimated from CIP and (a) GOES-10 and (b) GOES-12 for 31 July 2007.

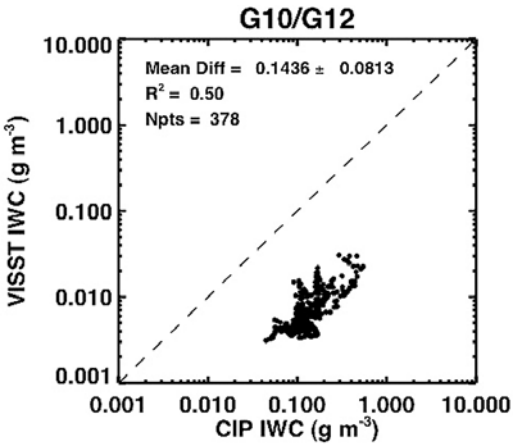

Figure 7. Scatterplot of IWC estimated from CIP and a combination of GOES-10/GOES-12 data for 31 July 2007.

GOES IWC values are fairly well correlated with a squared correlation coefficient $R^2 = 0.50$.

5.2. Image From 5 August 2007

[20] Figure 8 shows visible GOES imagery from 5 August 2007 at 1558 UTC. From 1445 to 1615 UTC, the ER-2 and DC-8 flew a coordinated path just south of the Gulf of Panama to obtain measurements of the properties of the anvils over that area. During this flight segment, the DC-8 maintained a fairly constant altitude near 12 km which was also near the level of complete attenuation of the CPL as shown in Figure 9a. For optically thick clouds, the VISST Z_{eff} closely matches the altitude at which complete beam attenuation occurs. When thin cirrus overlies another cloud layer, Z_{eff} is located between the two cloud layers. The difference between the GOES-10 and GOES-12 VZA was ~15° (Figure 9b) and the maximum VZA is ~25° so errors owing to pixel distortion should be small in this case as well. Again the in situ and GOES D_e follow similar trends with the largest particle sizes coinciding with optically thicker clouds (Figure 9c). The in situ and remotely sensed IWC values vary in the same way but are offset in magnitude (Figure 9d). The DC-8 was typically 2–3 km below cloud top where the cloud ice concentrations tend to be higher.

[21] Scatterplots of D_e for 5 August show more correlation than for the 31 July case (Figure 10). The mean differences between the CIP and GOES-10 and GOES-12 D_e values are less than 25 μm and are comparable to the previous case. The correlation is stronger here than in the previous case. For GOES-10 and GOES-12, $R^2 = 0.29$ and 0.40, respectively. A scatterplot of the in situ and remotely sensed IWC shows that CIP again generally finds larger IWC values (Figure 11). The mean difference is small, but unlike the previous case, the CIP and GOES IWC retrievals are nearly uncorrelated. The increased scatter may be due to errors in the retrieved Z_{eff}.

5.3. All Flight Days

[22] Much of the scatter in Figures 6, 7, 10, and 11 is partially a result of comparing measurements obtained by instruments with very different spatial resolutions and sampling schemes. GOES pixels have a nominal spatial resolution of 4 km at nadir while the CIP samples an extremely narrow swath along the path of the DC-8. Furthermore, the DC-8 often flew several kilometers below Z_{eff} and therefore potentially encountered very different cloud properties than those observed by space-based instruments. Because particle size and IWC can vary significantly on

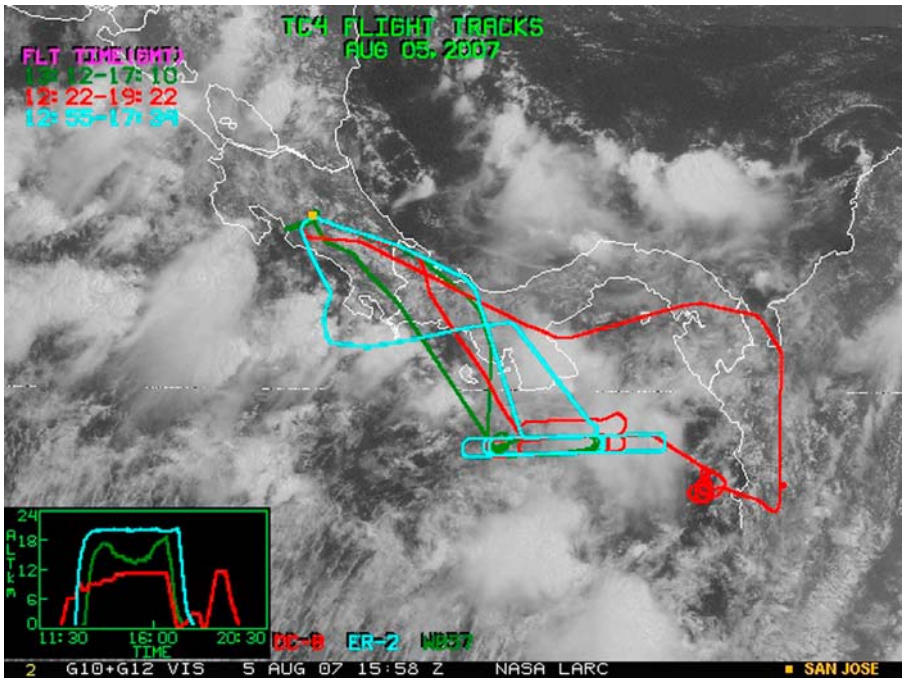

Figure 8. Composite GOES-10/GOES-12 visible image over the TC^4 domain at 1558 UTC on 5 August 2007. The flight tracks of the DC-8 and ER-2 are plotted over the image. Time series of the planes' altitudes are shown in the lower left inset.

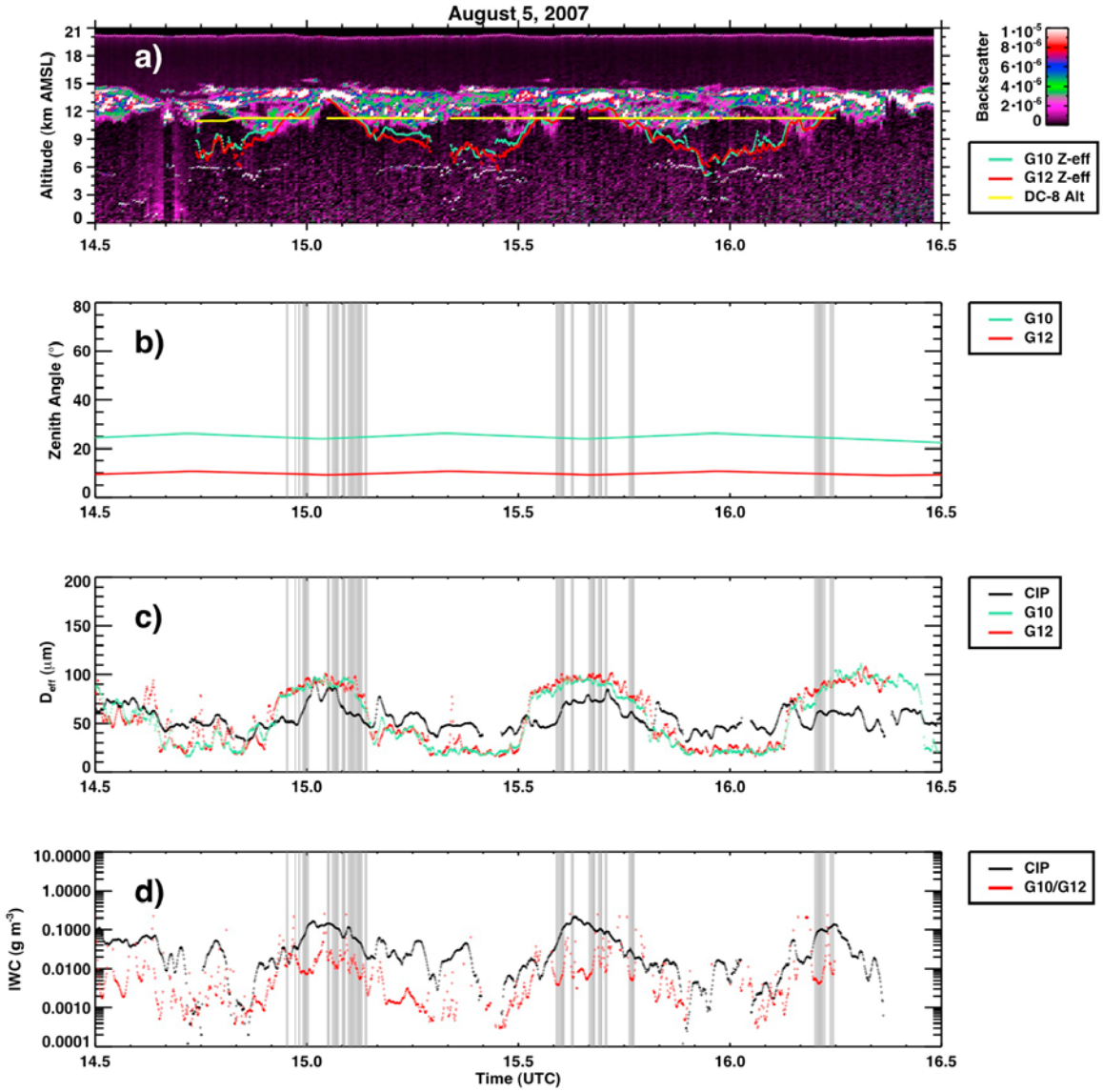

Figure 9. Time series of (a) cloud top, effective radiating, and aircraft altitude plotted over CPL 532 nm backscatter profiles; (b) satellite VZA; (c) effective ice crystal diameter; and (d) ice water content for 5 August 2007.

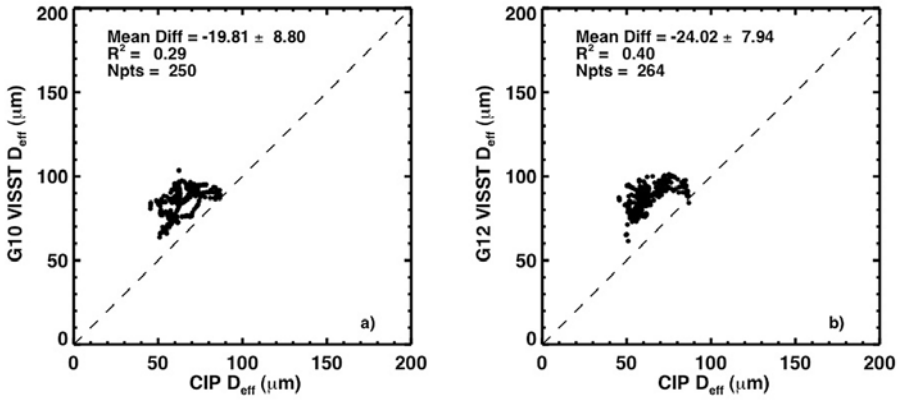

Figure 10. Scatterplots of D_e estimated from CIP and (a) GOES-10 and (b) GOES-12 for 5 August 2007.

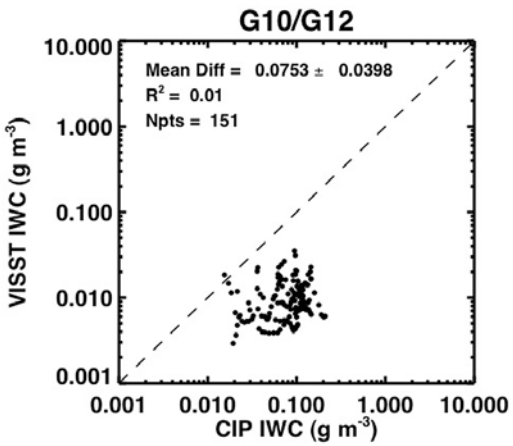

Figure 11. Scatterplot of IWC estimated from CIP and a combination of GOES-10/GOES-12 data for 5 August 2007.

small horizontal and vertical spatial scales, finding a meaningful way to validate space-based estimates of these cloud properties with in situ measurements is imperative and was one of the major science questions to be addressed by TC^4 [*Toon et al.*, 2010].

[23] Because the two different spatial resolutions of GOES and the CIP make comparison of instantaneous values of D_e and IWC difficult, a comparison of the mean properties is appropriate. The D_e values from CIP were binned according to the difference between the cloud top altitude observed by the CPL Z_{topCPL} and the altitude of the DC-8 Z_{DC8} using a 2 km bin size. The corresponding D_e values from VISST were binned in the same way. This procedure was performed for each of the flight days when there was a significant amount of coordination between the DC-8 and ER-2. Figure 12a shows the mean CIP and GOES D_e as a function of $Z_{topCPL} - Z_{DC8}$, where the midpoint of each 2 km bin is the abscissa. CIP values are represented by circles and the mean GOES-10/12 D_e are represented by squares. Coincidentally, the CIP and GOES mean D_e both increase with the DC-8 depth below cloud top and are well correlated (R^2 = 0.72). When $Z_{topCPL} - Z_{DC8} < 4$ km, the mean GOES D_e is larger than the CIP D_e while the opposite is true when $Z_{topCPL} - Z_{DC8} > 4$ km. When the DC-8 was near cloud top, the CIP was only sampling small particles while the satellite is sensitive to larger particles somewhat deeper in the cloud. Therefore, the mean D_e from CIP is smaller than the mean GOES D_e. At a certain depth below cloud top, in this case ~4 km, the DC-8 encountered larger ice particles from which the GOES satellites received very little or no signal. Therefore, the CIP D_e is larger than the GOES D_e. Despite the fact the GOES D_e represents an integrated quantity in the top few kilometers of the cloud, it seems to give an accurate representation, to within ~10 μm, of the in situ particle size.

[24] The same binning procedure described above in the particle size analysis was also carried out for IWC. The CIP measurements clearly demonstrate that mean IWC increases rapidly below cloud top (Figure 12b). The smallest difference between the mean GOES and CIP IWC is near cloud top where the difference between the means is 0.022 g m^{-3}. Below cloud top, IWC increases rapidly, while the satellite-retrieved IWC remains relatively constant since the GOES represents only the top few kilometers of the cloud.

[25] The same analysis was performed again for all DC-8 flights using Z_{eff} as the reference altitude instead of Z_{topCPL} and the results are shown in Figure 13. Note that although the DC-8 rarely flew above Z_{topCPL}, it occasionally flew above Z_{eff} as indicated by the negative values. The CIP mean D_e increases nearly monotonically from 60 to 180 μm over a depth of ~12 km (Figure 13a). The smallest particles are found close to cloud top ($Z_{eff} - Z_{DC8} = -5$). The GOES mean D_e are, of course, independent of the DC-8's altitude and show a less defined trend than the CIP retrievals. The best agreement between the CIP and GOES is attained when the DC-8 was near Z_{eff} itself (i.e., $Z_{eff} - Z_{DC8} = 0$) where the two means are within one standard deviation of each other. Note that the error bars for the CIP values become larger as $Z_{eff} - Z_{DC8}$ increases indicating that the ice crystal size distribution broadens with altitude beneath cloud top. Similarly, the GOES IWC means are closest to their CIP counterparts and within one standard deviation of each other above Z_{eff}, as expected (Figure 13b). The results in Figure 3b would suggest that the retrieved IWC should overestimate the CIP values above Z_{eff}. Unfortunately, most of those few data points from the DC-8 above Z_{eff} are just barely above Z_{eff} and, thus, are probably overestimates of the total column

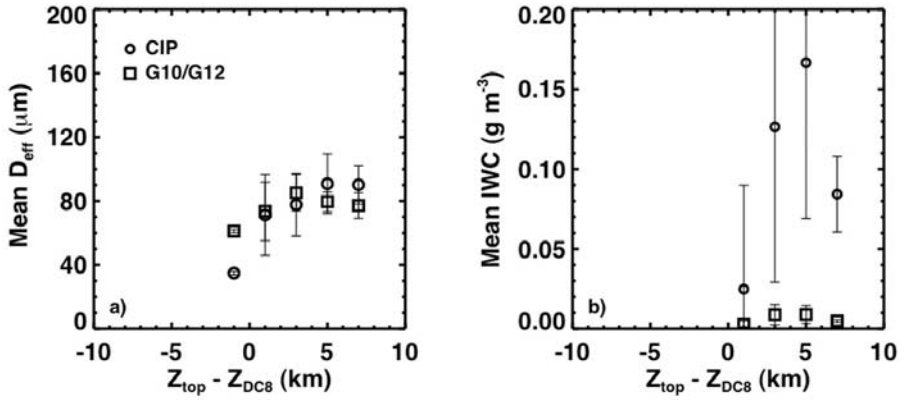

Figure 12. Mean (a) D_e and (b) IWC as a function of the vertical position of the DC-8 relative to the CPL Z_t for all coordinated flights with the DC-8 and ER-2.

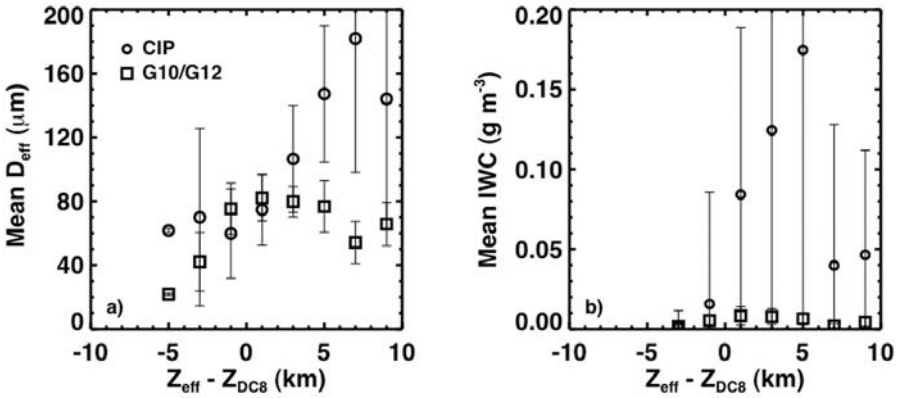

Figure 13. Mean (a) D_e and (b) IWC as a function of the vertical position of the DC-8 relative to Z_{eff} for all DC-8 flights. The bars indicate the standard deviations of the measurements.

above Z_{eff}. Like D_e, IWC exhibits increasing variability below cloud top.

5.4. Spirals

[26] The DC-8, with its array of cloud probes, has the unique ability to obtain vertical profiles of D_e and IWC by spiraling up or down through the entire depth of a cloud. On 24 July, the DC-8 executed an upward spiral near a developing convective core which eventually merged with another storm to the west (Figure 14). Starting around 1448 UTC the ascent was fairly gradual, taking about 35 min to complete (Figure 14a). Retrievals of Z_t, D_e, and IWC from GOES-10, GOES-12, and the CIP are summarized in Table 2. The CIP Z_t was located less than 1 km above that from both GOES retrievals. The CIP Z_t is taken to be the last altitude where measureable IWC was encountered and, because it is a single value, no standard deviation is given in Table 2. The D_e retrievals agree very well, ranging from 72.7 to 80.1 μm with standard deviations near 20 μm. Since the CIP measures IWC, integration over cloud depth is required to obtain IWP,

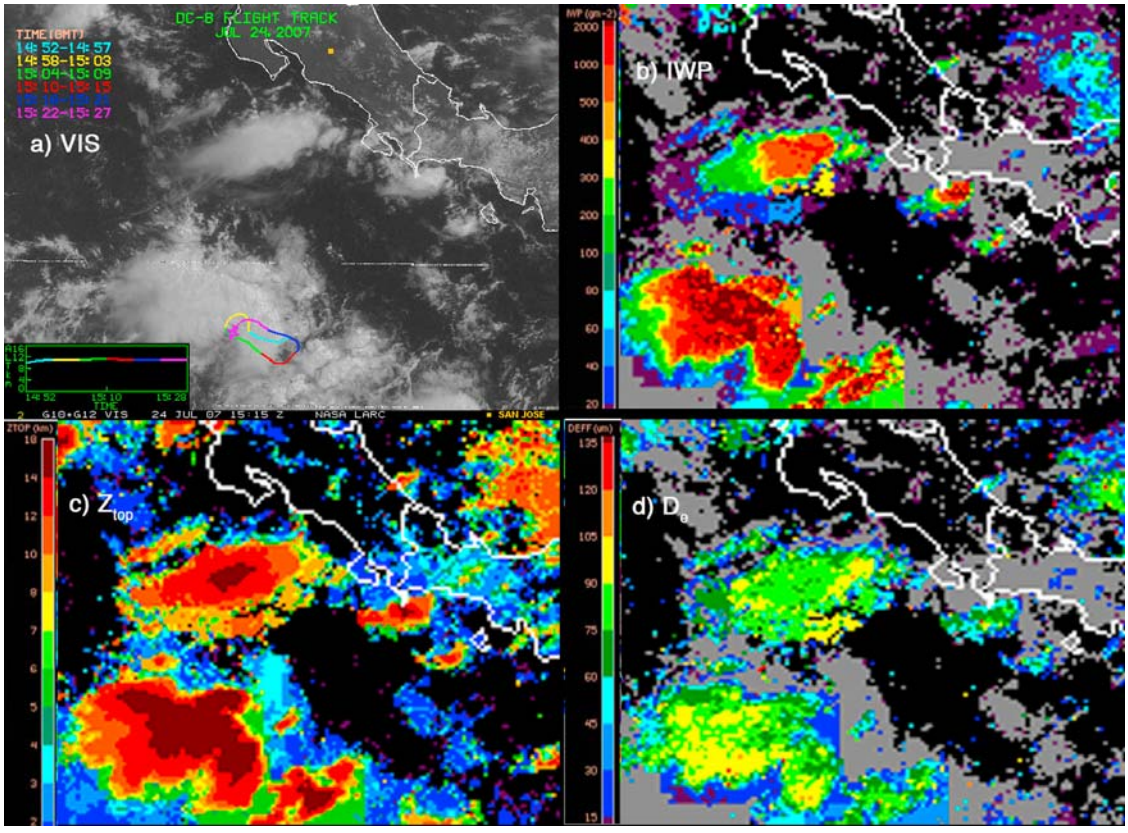

Figure 14. GOES-12 imagery and VISST cloud products for 1515 UTC on 24 July 2007. (a) VIS channel image with DC-8 flight track overlay, (b) IWP (gm^{-2}; gray areas indicate water clouds), (c) cloud-top height (km), and (d) D_e (μm).

Table 2. Satellite and in Situ Cloud Properties Derived From the DC-8 Spiral at ~1500 UTC on 24 July 2007

	GOES-10		GOES-12		CIP	
	Mean	SD	Mean	SD	Mean	SD
Z_t (km)	11.1	3.8	10.9	4.1	11.3	–
D_e (μm)	72.7	20.2	75.1	21.9	80.1	19.5
IWP (g m^{-2})	795.6	795.8	1260.4	1145.6	969.1	–

Table 3. Satellite and in Situ Cloud Properties Derived From the DC-8 Spiral at ~1705 UTC on 3 August 2007

	GOES-10		GOES-12		CIP	
	Mean	SD	Mean	SD	Mean	SD
Z_t (km)	12.2	0.6	12.3	0.7	11.6	–
D_e (μm)	73.0	14.5	90.8	33.6	87.4	46.7
IWP (g m^{-2})	186.2	101.9	277.0	188.2	328.6	–

which can then be compared to the GOES retrievals. Integration of IWC for this case yields IWP = 969 g m^{-2} and since it is a single value no standard deviation is given in Table 2. The CIP IWP is well within the range of 796–1260 g m^{-2} given by the GOES-10 and GOES-12 means. The GOES scanned this area twice, once at 1445 UTC and again at 1515 UTC, while the DC-8 was making its ascent. During this time, the cloud evolved considerably and the sampled scene was highly variable (Figures 14b–14d), which together explain why the GOES Z_t and IWP standard deviations are so high.

[27] Another spiral was performed on 3 August through a cirrus anvil over the Gulf of Panama (Figure 15). At 1705 UTC, the DC-8 began its descent from an altitude of 12 km, corresponding to cloud top. This spiral was completed in 19 min, about half the time of the previous case. As seen in Figure 15a, the spiral was conducted near the edge of the anvil where the variability in cloud properties (see Figures 15b–15d) were significant. GOES-10 scanned this area at 1658 and 1715 UTC and GOES-12 scanned at 1645 and 1715 UTC, but most of the pixels matched to the flight track came from the 1715 UTC scans. The CIP measurements indicate that ice crystals were detected down to 6 km which is taken to be cloud base. Table 3 summarizes the cloud properties obtained for this case. There is relatively good agreement between the DC-8 and GOES-derived cloud top heights with the former falling just within one standard deviation of the satellite values. Values of D_e are also fairly close especially for GOES-12. The CIP and GOES-12 mean values differ by only 4 μm, or 5%. The GOES-12 IWP value is well within one standard deviation, while GOES-10 seems to underestimate IWP. The difference between the CIP and GOES-12 values is 52 g m^{-2} or 15%.

[28] The differences between the parameter values from the two satellites in Tables 2 and 3 could be due to the model and structural differences noted earlier and perhaps to some small calibration and navigation differences. Figure 16 shows the histograms of IWP determined from the two satellites. They demonstrate the IWP variability among the pixels used in the comparisons. The primary peaks are nearly the same for both satellites during 24 July (Figure 16a) and 3 August (Figure 16b). However, the GOES-12 data show a greater spread in IWP for both cases. Part of the difference may be due to slightly smaller GOES-12 pixels capable of

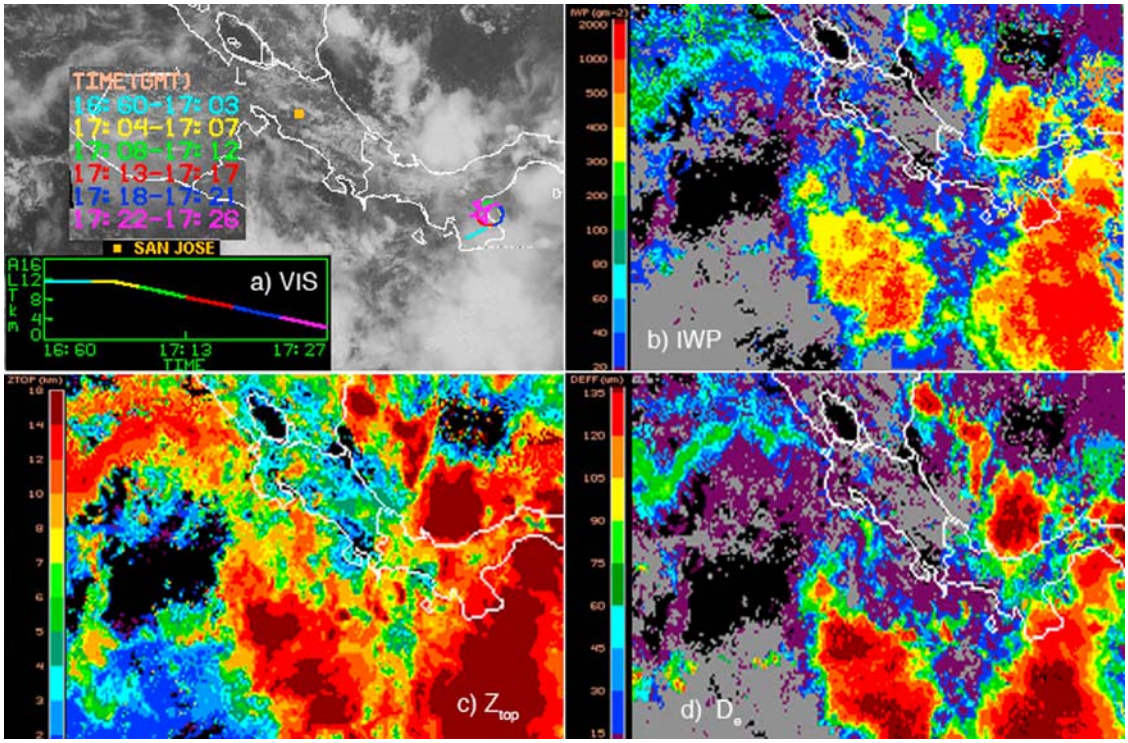

Figure 15. Same as Figure 14 except for 1715 UTC on 3 August 2007.

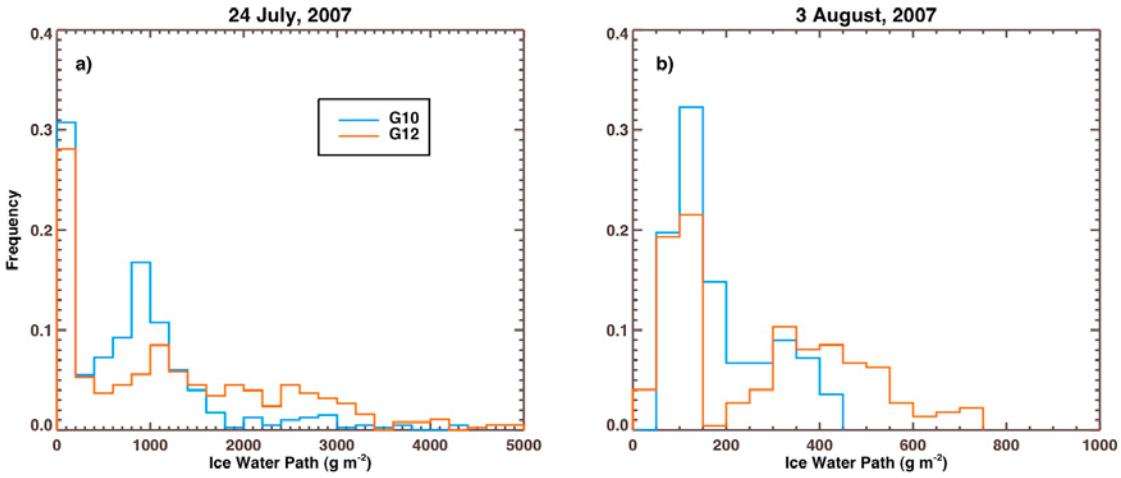

Figure 16. Histograms of retrieved IWP coinciding with the DC-8 spirals on (a) 24 July and (b) 3 August.

measuring smaller-scale variability. Additionally, the inherent structural differences of the cirrus clouds could include low-level clouds underneath the cirrus clouds because the CPL data were not available for screening. The low-level clouds observed by GOES-12 could be different from those seen by GOES-10 because of viewing angle differences. Such variability complicates comparisons among different satellites and in situ measurements. The results in Tables 2 and 3 are only two data points, but they are consistent with the other analyses in section 5.3. Altogether, within the limitations of the measurements, the comparisons indicate that the VISST retrievals of D_e, Z_t, and IWP, and by definition, τ, are representative of the anvil clouds over the TC^4 domain.

6. Summary and Future Work

[29] Careful analysis is required when comparing in situ and remotely sensed cloud properties because these quantities are often not directly comparable. In this study, estimates of D_e were computed from ice crystal size distributions collected by the CIP aboard the DC-8 aircraft and compared to GOES retrievals matched in space and time. A new method to estimate IWC near cloud top with coincident satellite observations was developed and the resulting values were compared with in situ measurements taken by the CIP. Instantaneous comparisons of both D_e and IWC show significant differences although there is some correlation between the in situ and remotely sensed properties. On average, the D_e retrievals from GOES are an accurate representation of the in situ particle size as measured by the CIP. The two comparisons with the CIP-derived IWPs indicate that the GOES-retrieved ice water path is a reasonable representation of the scene. These results are consistent with other comparisons [*Mace et al.*, 2005; *Waliser et al.*, 2009], which show that the VISST, on average, provides accurate estimates of IWP. The results are encouraging for using the new method for retrieving cloud top IWC using dual-angle views. While the mean GOES-retrieved IWC is in agreement with its DC-8 counterpart near cloud top, the IWC increases rapidly with decreasing height in the cloud. The results, for at least one flight, show that the IWC near cloud top is related to that deeper in the cloud. If that correlation is common, then it becomes more likely that reasonably accurate profiles of D_e and IWC below cloud top can be estimated from passive satellite observations alone, especially if additional spectral information is available [e.g., *Wang et al.*, 2009].

[30] Knowledge of the vertical profiles of particle size and IWC are important for validating, initializing, and improving cloud process and other less sophisticated weather and climate models that explicitly include cloud microphysical properties. Thus, accurate retrievals of those quantities from geostationary satellite data should be valuable for improving numerical weather analyses and forecasts. The retrievals could also be valuable for aviation safety. Areas of large concentrations of ice (IWC > 1 g m^{-3}) in convective cloud systems pose a threat to aviation because ingest of too much ice in a jet engine can induce engine rollback and failure [*Lawson et al.*, 1998; *Mason et al.*, 2006]. If techniques can be developed to detect areas of potentially high IWC, it may be possible to provide warnings to air traffic controllers so that such incidents can be avoided. A correlation between IWC at cloud top and the IWC deeper in the cloud may be the basis for such a technique. The approach developed in this paper requires two satellites, or, at least, two different viewing zenith angles to retrieve IWC near cloud top. Thus, it would be practical for application over much of North America, which is viewed by two GOES, or for any other region where the satellite images overlap within a few minutes of each other. When the new GOES-R series of imagers [*Schmit et al.*, 2005] become available later in this decade, the extra channels needed to estimate the vertical profile of D_e will be available and the technique could be further refined.

[31] The results presented here represent only a first step in retrieving cloud top IWC from passive satellite data. Much additional research is required to validate and improve the technique and to define its limits. The validation here was limited by the DC-8's ceiling. In situ measurements taken throughout the anvil cloud are needed. Similarly, additional validations of the retrieved values of D_e and IWP are required to establish reliable uncertainty

bounds. Those validations will require extensive comparisons with data from instruments such as those on CloudSat and CALIPSO and at the Atmospheric Radiation Measurement Program sites [*Ackerman and Stokes*, 2003]. Comparisons with in situ measurements in various conditions will also be necessary for complete evaluation of the retrievals. Such efforts are currently ongoing.

[32] **Acknowledgments.** This research was supported by the NASA Applied Sciences Program, the Department of Energy Atmospheric Radiation Measurement Program through Interagency Agreement DE-AI02-07ER64546, and the NOAA Center for Satellite Applications and Research GOES-R Program.

References

Ackerman, T. P., and G. Stokes (2003), The Atmospheric Radiation Measurement Program, *Phys. Today*, *56*, 38–45, doi:10.1063/1.1554135.

Benjamin, S. G., S. S. Weygandt, J. M. Brown, T. L. Smith, T. G. Smirnova, W. R. Moninger, B. Schwartz, E. J. Szoke, and K. Brundage (2004), Assimilation of METAR cloud and visibility observations in the RUC, 11th Conf. on Aviation, Range, Aerospace Meteorology (ARAM) and 22nd Conf. on Severe Local Storms, Hyannis, Mass., Am. Meteorol. Soc., 9.13.

Chang, F.-L., P. Minnis, B. Lin, M. M. Khaiyer, R. Palikonda, and D. A. Spangenberg (2010), A modified method for inferring upper troposphere cloud top height using the GOES 12 imager 10.7 and 13.3 μm data, *J. Geophys. Res.*, *115*, D06208, doi:10.1029/2009JD012304.

Coakley, J. A., Jr., and R. Davies (1986), The effect of cloud sides on reflected solar radiation as deduced from satellite observations, *J. Atmos. Sci.*, *43*, 1025–1035, doi:10.1175/1520-0469(1986)043<1025:TEOCSO>2.0.CO;2.

Dong, X., G. G. Mace, P. Minnis, W. L. Smith Jr., M. Poellot, R. T. Marchand, and A. D. Rapp (2002), Comparison of stratus cloud properties deduced from surface, GOES, and aircraft data during the March 2000 ARM cloud IOP, *J. Atmos. Sci.*, *59*, 3265–3284, doi:10.1175/1520-0469(2002)059<3265:COSCPD>2.0.CO;2.

Garrett, T. J., et al. (2005), In situ measurements of the microphysical and radiative evolution of a Florida cirrus anvil, *J. Atmos. Sci.*, *62*, 2352–2372, doi:10.1175/JAS3495.1.

Kingsmill, D. E., et al. (2004), TRMM common microphysics products: A tool for evaluating spaceborne precipitation retrieval algorithms, *J. Appl. Meteorol.*, *43*, 1598–1618, doi:10.1175/JAM2151.1.

Lawson, R. P., L. J. Angus, and A. J. Heymsfield (1998), Cloud particle measurements in thunderstorm anvils and possible weather threat to aviation, *J. Aircr.*, *35*, 113–121, doi:10.2514/2.2268.

Mace, G. G., Y. Zhang, S. Platnick, M. D. King, P. Minnis, and P. Yang (2005), Evaluation of cirrus cloud properties from MODIS radiances using cloud properties derived from ground-based data collected at the ARM SGP site, *J. Appl. Meteorol.*, *44*, 221–240, doi:10.1175/JAM2193.1.

Mason, J. G., J. W. Strapp, and P. Chow (2006), The ice particle threat to engines in flight, paper presented at the 44th AIAA Aerospace Sciences Meeting and Exhibit, Am. Inst. Aeronaut. and Astronaut., Reno, Nev., 9–12 Jan.

McGill, M., D. Hlavka, W. Hart, V. S. Scott, J. Spinhirne, and B. Schmid (2002), Cloud physics lidar: Instrument description and initial measurement results, *Appl. Opt.*, *41*, 3725–3734, doi:10.1364/AO.41.003725.

Minnis, P., D. P. Garber, D. F. Young, R. F. Arduini, and Y. Takano (1998), Parameterization of reflectance and effective emittance for satellite remote sensing of cloud properties, *J. Atmos. Sci.*, *55*, 3313–3339, doi:10.1175/1520-0469(1998)055<3313:PORAEE>2.0.CO;2.

Minnis, P., C. R. Yost, S. Sun-Mack, and Y. Chen (2008), Estimating the physical top altitude of optically thick ice clouds from thermal infrared satellite observations using CALIPSO data, *Geophys. Res. Lett.*, *35*, L12801, doi:10.1029/2008GL033947.

Schmit, T. J., M. M. Gunshor, W. P. Menzel, J. Li, S. Bachmeier, and J. J. Gurka (2005), Introducing the next-generation Advanced Baseline Imager (ABI) on GOES-R, *Bull. Am. Meteorol. Soc.*, *86*, 1079–1096, doi:10.1175/BAMS-86-8-1079.

Seo, E. K., and G. Liu (2006), Determination of 3D cloud ice water contents by combining multiple data sources from satellite, ground radar, and a numerical model, *J. Appl. Meteorol. Climatol.*, *45*, 1494–1504, doi:10.1175/JAM2430.1.

Sherwood, S. C., J.-H. Chae, P. Minnis, and M. McGill (2004), Underestimation of deep convective cloud tops by thermal imagery, *Geophys. Res. Lett.*, *31*, L11102, doi:10.1029/2004GL019699.

Stamnes, K., S. C. Tsay, W. Wiscombe, and K. Jayaweera (1988), Numerically stable algorithm for discrete-ordinate-method radiative transfer in multiple scattering and emitting layered media, *Appl. Opt.*, *27*, 2502–2509, doi:10.1364/AO.27.002502.

Stephens, G. L., et al. (2008), CloudSat mission: Performance and early science after the first year of operation, *J. Geophys. Res.*, *113*, D00A18, doi:10.1029/2008JD009982.

Toon, O. B., et al. (2010), Planning, implementation, and first results of the Tropical Composition, Cloud Climate Coupling Experiment (TC^4), *J. Geophys. Res.*, *115*, D00J04, doi:10.1029/2009JD013073.

Waliser, D. E., et al. (2009), Cloud ice: A climate model challenge with signs and expectations of progress, *J. Geophys. Res.*, *114*, D00A21, doi:10.1029/2008JD010015.

Wang, Z., and K. Sassen (2002), Cirrus cloud microphysical property retrieval using lidar and radar measurements. part I: Algorithm description and comparison with in situ data, *J. Appl. Meteorol.*, *41*, 218–229, doi:10.1175/1520-0450(2002)041<0218:CCMPRU>2.0.CO;2.

Wang, X., K. N. Liou, S. C. Ou, G. G. Mace, and M. Deng (2009), Remote sensing of cirrus vertical size profile using MODIS data, *J. Geophys. Res.*, *114*, D09205, doi:10.1029/2008JD011327.

Winker, D. M., W. H. Hunt, and M. J. McGill (2007), Initial performance assessment of CALIOP, *Geophys. Res. Lett.*, *34*, L19803, doi:10.1029/2007GL030135.

Wyser, K., and P. Yang (1998), Average ice crystal size and bulk shortwave single-scattering properties of cirrus clouds, *Atmos. Res.*, *49*, 315–335, doi:10.1016/S0169-8095(98)00083-0.

Yang, P., B. A. Baum, A. J. Heymsfield, Y. X. Hu, H.-L. Huang, S.-C. Tsay, and S. Ackerman (2003), Single-scattering properties of droxtals, *J. Quant. Spectrosc. Radiat. Transfer*, *79-80*, 1159–1169, doi:10.1016/S0022-4073(02)00347-3.

J. K. Ayers, D. A. Spangenberg, and C. R. Yost, Science Systems and Applications, Inc., 1 Enterprise Pkwy., Ste. 200, Hampton, VA 23666, USA. (christopher.r.yost@nasa.gov)

A. Bansemer and A. J. Heymsfield, National Center for Atmospheric Research, P.O. Box 3000, Boulder, CO 80307, USA.

D. L. Hlavka, Science Systems and Applications, Inc., Code 912, Greenbelt, MD 20771, USA.

M. J. McGill, NASA Goddard Space Flight Center, Code 613.1, Greenbelt, MD, USA.

P. Minnis, NASA Langley Research Center, MS 420, Hampton, VA 23681-0001, USA.